Journal of Solid State Chemistry 184 (2011) 1989–1996

Contents lists available at ScienceDirect

Journal of Solid State Chemistry

journal homepage: www.elsevier.com/locate/jssc

Phase-controlled solvothermal synthesis and characterization of nickel sulfides with good single crystalline nature

Shuguang Chen*, Kai Zeng, Haibin Li, Fujin Li

School of Physics and Electronic Science, Changsha University of Science and Technology, Changsha 410114, People's Republic of China

ARTICLE INFO

Article history:
Received 3 February 2011
Received in revised form
23 May 2011
Accepted 29 May 2011
Available online 6 June 2011

Keywords:
Nickel sulfide
Solvothermal
Crystal structure
Crystal growth

ABSTRACT

Dispersed rhombohedral NiS rods with high aspect ratios and rhombic dodecahedron-like cubic NiS_2 crystals were prepared by solvothermal routes using $NiCl_2 \cdot 6H_2O$ and $Na_2S_2O_3 \cdot 5H_2O$ as reagents and ethylenediamine as a solvent, and 3D blossoming flower-like rhombohedral NiS microstructures were synthesized using different sulfur sources of thiourea. The products were characterized by X-ray diffraction, field emission scanning electron microscopy, transmission electron microscopy, energy dispersion spectrometry and selected area electronic diffraction. All the products were pure and had good single crystalline nature. The synthesis parameters were of great importance on the purity and morphology of the products. The possible growth mechanisms have been discussed based on the analyses of the effects of sulfur sources and solvent on the crystal structures and detailed configurations of the products. The present work is likely to help the phase-controlled synthesis of other metal chalcogenides.

1. Introduction

Due to their structurally and dimensionally dependent physical properties and potential applications, inorganic materials with controlled crystal structures, shapes and sizes have drawn extensive attention in the field of materials science [1,2]. As members of semiconductor-related materials, nickel sulfides in different stoichiometries are used widely as hydrodesulfurization catalysts [3,4], cathode materials in rechargeable lithium batteries [5–7] and materials in paramagnetic–antiferromagnetic phase transition [8,9] and they have drawn extensive attention of researchers to prepare them with special morphologies and shapes [10–31]. Among the numerous researchers, Qian's group achieved prodigious success in synthesizing nickel sulfides, and rhombohedral NiS (r-NiS) nanoparticles [15], nanorods [18] and microspheres [28], hexagonal NiS (h-NiS) nanobelts [11], r-NiS with urchin-like 3D nanostructures [17] and NiS_2 microspheres and nanoparticles. Moreover, interesting morphologies such as carnation-like r-NiS microspheres [14], r-NiS triangular nanoprisms [16], hollow h-NiS nanospheres [21], chain-like r-NiS tubes and echinus-like Ni_3S_2 nanostructures [26] and cubic pyrite NiS_2 dodecahedrons [30,31] are reported. Except for the syntheses of single crystalline r-NiS crystals reported in Refs. [17,18,27], the majority of r-NiS crystals and NiS_2 crystals reported previously are of polycrystalline nature [10–12,14,15,22,24,31] or not pure [13,16].

In this work, r-NiS dispersed rods with high aspect ratios, 3D blossoming flower-like r-NiS microstructures and homogeneous rhombic dodecahedron-like NiS_2 crystals are synthesized via simple solvothermal routes using ethylenediamine (en) as a solvent. All the obtained products are pure and have good single crystalline nature. We present an approach based on XRD analysis to the phase-controlled synthesis of nickel sulfides. XRD analysis is applied to evaluate the effects of molar ratio of Ni to S, reaction time and temperature on phase purity of the products. The reaction conditions for the synthesis of pure r-NiS are put forward based on the XRD analysis, which is proved by the experiments. Such an approach may find application in phase-controlled synthesis of other metal chalcogenides. Furthermore, to the best of our knowledge, it is for the first time that r-NiS rods with equilateral triangle-like cross-sections are reported. We analyze the preferential orientation of r-NiS rods and formation mechanisms of equilateral triangle-like cross-sections using HRTEM and SAED, which may provide some useful ideas for the discussion of the formation mechanism of crystals. In addition the electrochemical properties of the obtained single crystalline r-NiS and NiS_2 crystals are investigated in the present work, which have not been reported previously [5–7].

2. Experimental section

2.1. Synthesis of r-NiS and NiS_2 microstrctures

All analytical chemicals were used without further purification. In a typical procedure, 0.002 mol $NiCl_2 \cdot 6H_2O$ was added to 40 mL

* Corresponding author. Fax: +86 731 85258217.
E-mail address: hustcsg@sohu.com (S. Chen).

0022-4596/$ - see front matter © 2011 Elsevier Inc. All rights reserved.
doi:10.1016/j.jssc.2011.05.055

ethylenediamine with intensive stirring to form opaque slurry containing purple precipitates; then a sulfur source, $Na_2S_2O_3 \cdot 5H_2O$ or thiourea, with different molar ratios to $NiCl_2 \cdot 6H_2O$ was added to the slurry with intensive stirring to form homogeneous opaque mixtures; subsequently the obtained mixtures were transferred to a Teflon-lined stainless steel autoclave with a capacity of 50 mL. After that the autoclave was heated at a certain reaction temperature for a certain time and subsequently cooled naturally to room temperature. Finally the precipitates were washed several times with distilled water and ethanol, dried at 120 °C for 12 h and products were obtained.

2.2. Characterization

Products were characterized by X-ray powder diffraction (XRD) on a Rigaku D/max 2200 diffractionmeter with a graphite monochromator and Cu$K\alpha$ radiation ($\lambda = 1.5406$ Å) at a scanning speed of 4°/min. Scanning electron microscopy (SEM) images were observed by a LEO 1525 field emission scanning electron microscopy (FESEM). The compositions of the products were measured on an Oxford link-ISIS 300 energy dispersion spectrometer (EDS). High resolution transmission electron microscopy (HRTEM) images and selected area electronic diffraction (SAED) patterns were obtained on a JEOL JEM-3010 unit.

2.3. Experiments for electrochemical properties

To fabricate the NiS or NiS_2 electrodes 80 wt% NiS or NiS_2 was mixed with 10 wt% carbon black and 10 wt% polyvinylidene fluoride (PVDF) binder, using N-methyl-2-pyrrolidinone (NMP) as a dispersant to form a slurry. The slurry was spread on aluminum foil substrates. After drying under vacuum, the electrodes were cut into circular foils with a diameter of 10 mm. CR2025 coin-type cells were assembled in an argon-filled glove box using lithium metal foil as the counter electrode. The electrolyte was 1 M $LiPF_6$ in a mixture of ethylene carbonate (EC) and dimethyl carbonate (DMC; 1:1 by volume). The cells were galvanostatically charged and discharged at room temperature in the range of 1.0–3.0 V at 0.1 C (1 C = 590 mA h/g).

3. Results and discussion

3.1. XRD analysis

Fig. 1a1 shows the XRD patterns of the products synthesized from $Na_2S_2O_3 \cdot 5H_2O$ when the mole ratio of $Na_2S_2O_3$ to $NiCl_2$ is 2. Little r-NiS (JCPDS No. 862281) is obtained when the temperature is under 200 °C, and the contents of r-NiS in the products increase with temperature increment. With time extension the contents of cubic NiS_2 (JCPDS No. 893058) in the products synthesized at 215 °C exhibit a trend of increase first and drop subsequently, and NiS_2 is converted to r-NiS gradually. However, pure r-NiS cannot be obtained at 215 °C even if the reaction time is extended to 120 h. In order to synthesize pure r-NiS, the effects of temperature, time and mole ratio of $Na_2S_2O_3$ to $NiCl_2$ on the phase compositions are investigated. The contents of r-NiS in the products synthesized under different conditions are calculated and shown in Fig. 1a2. In calculation the integral areas of the diffraction peaks, (3 0 0) of r-NiS and (2 0 0) of NiS_2 of the corresponding XRD patterns, and RIR values of r-NiS (2.31) and NiS_2 (3.19) are taken into account. Here, the RIR value gives the intensity ratio of the strongest diffraction peaks of the target material to corundum when both are mixed with equal weight. It can be concluded from the results that pure r-NiS can be obtained after reaction for a long time when the temperature is higher than 215 °C and especially the mole ratio of $Na_2S_2O_3$ to $NiCl_2$ is close to 1.925. Well-crystallized pure r-NiS (Fig. 1a3) is synthesized at 225 °C for 120 h when the mole ratio of $Na_2S_2O_3$ to $NiCl_2$ is 1.925, which is in accordance with the results deduced from Fig. 1a2. As for NiS_2 pure products can be easily obtained above 200 °C when the mole ratio of $Na_2S_2O_3$ to $NiCl_2$ is above 3, which is proved by Fig. 1a2 and 1a4. It can be also found from Fig. 1a4 that some NiS_2 transforms to r-NiS with time extension at temperature higher than 215 °C. Moreover, elemental S appears when the reaction is carried out at 180 °C for 20 h.

Fig. 1b shows the XRD patterns of the products synthesized from thiourea at 200 °C when the mole ratio of thiourea to $NiCl_2$ is 2, and it is found that a small quantity of h-NiS (JCPDS No. 891957) exists at relatively short reaction time. In fact, in spite of the different mole ratios of thiourea to $NiCl_2$, no product is obtained when the temperature is under 180 °C, and well-crystallized pure r-NiS can be synthesized under conditions of temperature higher than 200 °C and reaction time longer than 60 h. However, the yields of r-NiS increased with an increment of the mole ratio of thiourea to $NiCl_2$ at the same dosage of $NiCl_2 \cdot 6H_2O$. Though Meng et al. [28] used the same method to synthesize r-NiS they found that the molar ratio of S to Ni has no effect on phase structure; they perhaps ignored the existence of a small quantity of h-NiS and the phase transformation from h-NiS to r-NiS.

3.2. SEM analysis

The SEM images of products synthesized under different conditions are presented in Fig. 2. It can be seen from Fig. 2a that r-NiS powders synthesized from $Na_2S_2O_3 \cdot 5H_2O$ consist almost entirely of dispersed rods, most of which have cross-sectional diameters of 1–4 μm and high aspect ratios of 20–80. Shen et al. [24] synthesized r-NiS nanorods of similar shapes at 165 °C with the help of hydrazine hydrate. However, we cannot obtain rod-like r-NiS at such low temperature due to the absence of hydrazine hydrate. NiS_2 powders (Fig. 2b) synthesized from $Na_2S_2O_3 \cdot 5H_2O$ are fine and homogeneous rhombic dodecahedron-like particles with a mean size of 2 μm, and the rhombic dodecahedron is constructed by twelve equivalent rhombuses with two acute angles of 70.5° and two obtuse angles of 109.5°. NiS_2 powders with similar morphologies have been produced by Yu and Yoshimura [30] and Yang et al. [31] using elemental S as the sulfur source. Typical SEM image of r-NiS synthesized from thiourea is shown in Fig. 2c. Large quantity of novel 3D blossoming flower-like crystals is obtained, and each 3D microstructure is composed of ray-like rods growing from a core. Pan et al. [25] and Liu [27] obtained analogous architectures using thiourea, which show significant differences from our work in detailed shapes. Moreover rods with equilateral triangle-like cross section are observed as shown by the arrows in the inset of Fig. 2a and c, which has not been reported in the previous work.

3.3. TEM observation

Fig. 3a1 and a2 shows HRTEM images and SAED patterns of r-NiS synthesized from $Na_2S_2O_3 \cdot 5H_2O$. The strong and well-arrayed SAED spots indicate the single crystalline nature of r-NiS crystals. The crystallographic planes indexed in HRTEM are in good accordance with the results of SAED. According to the corresponding TEM images and SAED patterns obtained by projecting two different diffraction beams along $[\bar{1}\,1\,1]$ and $[1\,8\,\bar{4}]$ crystallographic orientation it can be found that *c*-axis, namely [0 0 1] crystallographic orientation, and the axial direction of r-NiS rods are coplanar. It indicates that the axial direction of r-NiS rod is parallel to *c*-axis. The same results are obtained

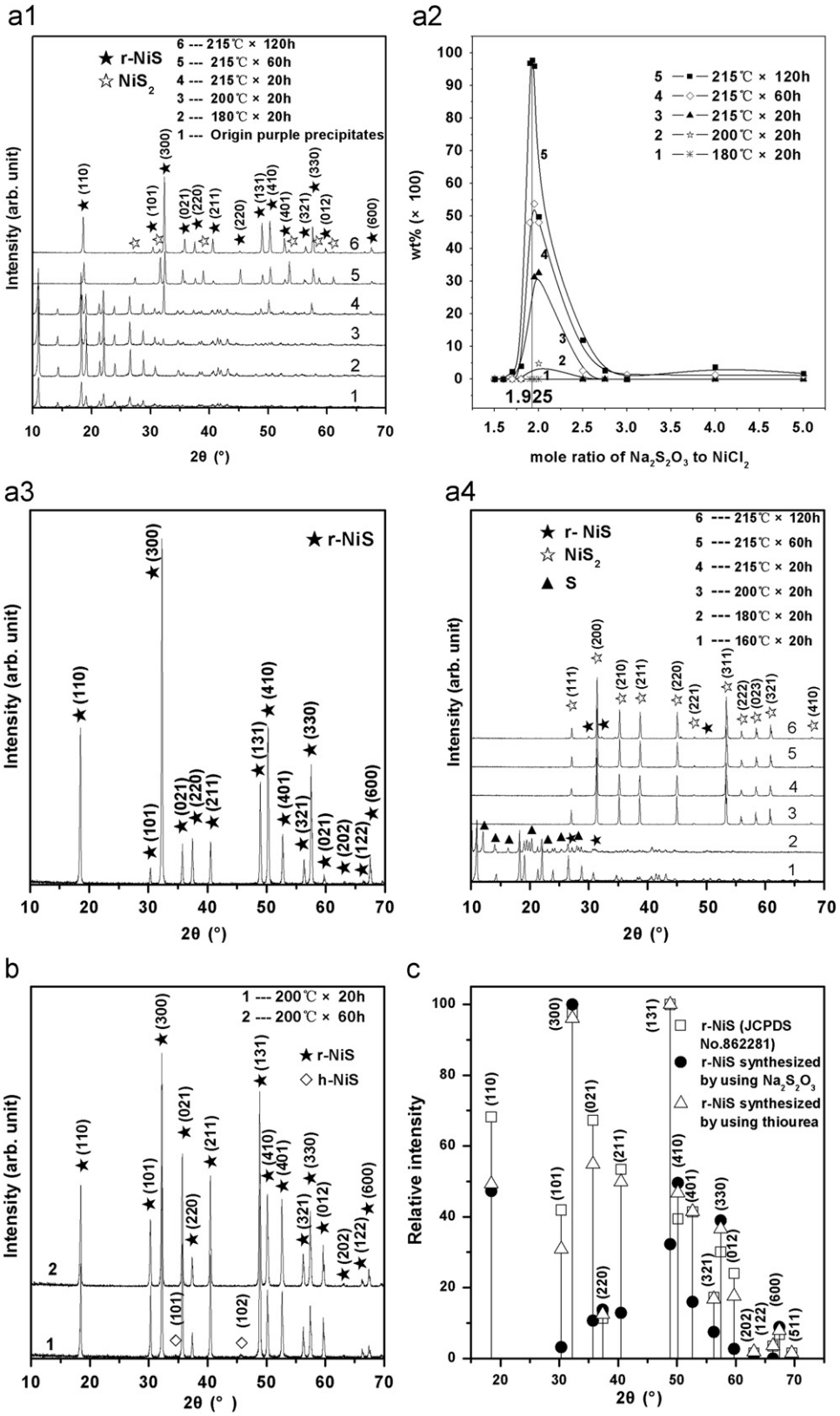

Fig. 1. (a1) XRD patterns of the products synthesized from $Na_2S_2O_3 \cdot 5H_2O$ when the mole ratio of $Na_2S_2O_3$ to $NiCl_2$ is 2; (a2) the contents of r-NiS in the products synthesized from $Na_2S_2O_3 \cdot 5H_2O$ when the mole ratio of $Na_2S_2O_3$ to $NiCl_2$ varies from 1.5 to 5; (a3) XRD pattern of the products synthesized from $Na_2S_2O_3 \cdot 5H_2O$ at 225 °C for 120 h when the mole ratio of $Na_2S_2O_3$ to $NiCl_2$ is 1.925; (a4) XRD patterns of the products synthesized from $Na_2S_2O_3 \cdot 5H_2O$ when the mole ratio of $Na_2S_2O_3$ to $NiCl_2$ is 5; (b) XRD patterns of the products synthesized from thiourea when the mole ratio of thiourea to $NiCl_2$ is 2; (c) relative intensities of the diffraction peaks of pure r-NiS deduced from the standard reflection of JCPDS No. 862281 and the XRD patterns of (a3) and (b).

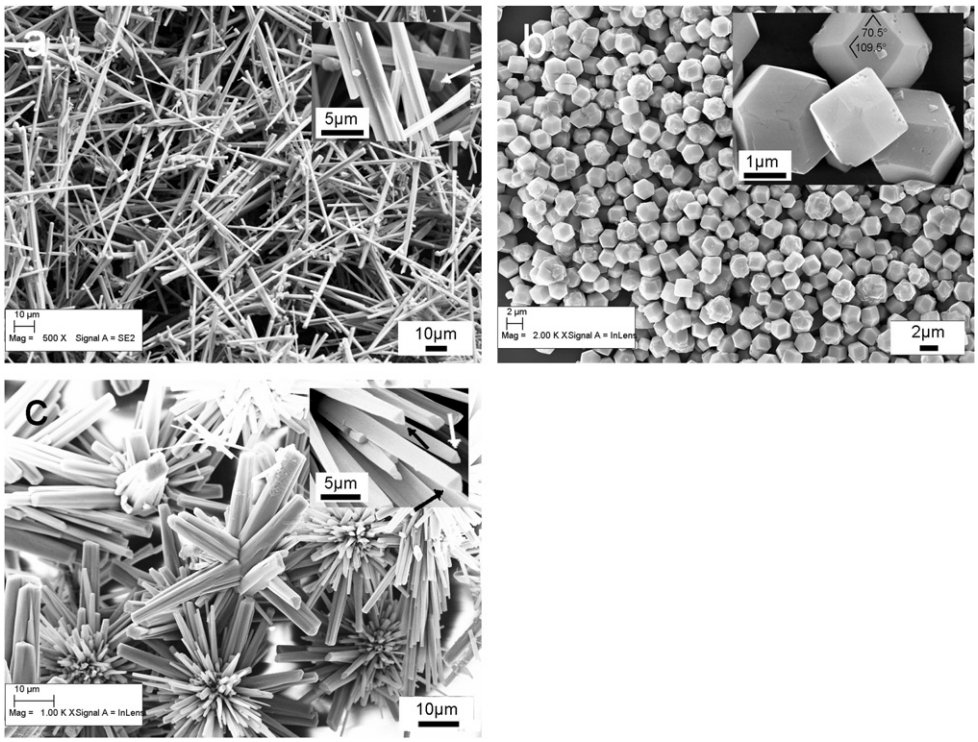

Fig. 2. (a) SEM image of r-NiS synthesized at 225 °C for 120 h when the mole ratio of $Na_2S_2O_3$ to $NiCl_2$ is 1.925; (b) SEM image of NiS_2 synthesized at 200 °C for 20 h when the mole ratio of $Na_2S_2O_3$ to $NiCl_2$ is 5; (c) SEM image of r-NiS synthesized at 200 °C for 60 h using thiourea when its mole ratio to $NiCl_2$ is 2. The insets show the local and detailed configurations of corresponding images.

from Fig. 3b1 and b2. It proves that the rods growing from the core of r-NiS synthesized from thiourea are of single crystalline nature, and the axial direction of each rod is parallel to the *c*-axis. Similarly, NiS_2 rhombic dodecahedron-like crystals show single crystalline nature. It can be seen in Fig. 3c that the surface perpendicular to the paper and in the upper-right corner is perpendicular to [1 1 0] crystallographic orientation, which is in good agreement with the theoretical analysis results put forward by Yu and Yoshimura [30] and Yang et al. [31]. Since the majority of r-NiS rods synthesized from $Na_2S_2O_3 \cdot 5H_2O$ prefer an orientation parallel to the plane of the sample for XRD measurement and the axial direction of each rod is parallel to the *c*-axis, the relative intensities of certain diffraction peaks in Fig. 1c show significant difference from the standard reflection of JCPDS No. 862281. Such diffraction peaks as (1 0 1), (0 2 1) and (2 1 1) form relatively large angles of 69.29°, 52.90°and 37.36° with *c*-axis, respectively, resulting in the difference in relative diffraction intensities and proving the single crystalline nature. It is interesting that Shen et al. [24] obtained r-NiS with similar morphologies. However, the XRD pattern of such products is consistent with the standard reflection of JCPDS No. 862281. It may be attributed to the polycrystalline nature of these products. In addition the differences between the XRD results of r-NiS synthesized from thiourea and JCPDS no. 862281 are illegible, which is ascribed to the 3D blossoming flower-like structure resulting in similar XRD patterns to those of polycrystalline powders.

3.4. Growth mechanism

To understand the growth mechanisms of the products synthesized from $Na_2S_2O_3 \cdot 5H_2O$ and thiourea, the intermediate products synthesized at relatively short reaction time are prepared. Fig. 4a shows the SEM image of the products synthesized at 225 °C for 20 h when the mole ratio of $Na_2S_2O_3$ to $NiCl_2$ is 1.925. EDS analyses of Spots A and B in Fig. 4a reveal that nickel–sulfur molar ratio is about 1:1, and that of Spots C and D in Fig. 4a is about 1:2. It indicates the coexistence of r-NiS rods and NiS_2 rhombic dodecahedron-like crystals. The products synthesized at 200 °C for 4 h when the mole ratio of $Na_2S_2O_3$ to $NiCl_2$ is 5 are black purple, and it is easy to find bigger particles in the SEM image (Fig. 4b). EDS analyses of Spots E and F in Fig. 4b reveal nickel–sulfur molar ratio of about 2:1, which proves the synthesis of NiS_2 crystals. EDS analyses of Spots G and H in Fig. 4b reveal that the relatively small particles contain chlorine element, indicating that such particles are originally purple precipitates—nickel complex of $[Ni(en)_3]Cl_2$ [18]. The black purple color should be attributed to the coexistence of the purple $[Ni(en)_3]Cl_2$ precipitates and black NiS_2 crystals. In addition the SEM image (Fig. 4c) discloses that a large quantity of 3D intersecting rods is formed at relatively short reaction time, and the cross-sections of the rods present fine equilateral triangle-like morphologies.

Based on the results mentioned above, we propose the possible growth mechanisms of different products. Purple $[Ni(en)_3]Cl_2$ precipitates are formed at the beginning of reaction, $Na_2S_2O_3 \cdot 5H_2O$ first decomposes to Na_2SO_3 and S upon heating and then Na_2SO_3 is further converted to Na_2S and Na_2SO_4 through a disproportionation process. So the reaction processes of the products synthesized from $Na_2S_2O_3 \cdot 5H_2O$ can be described by as follows:

$$NiCl_2 \cdot 6H_2O + 3en \rightarrow [Ni(en)_3]Cl_2 \downarrow (purple) + 6H_2O \quad (1)$$

$$4S_2O_3^{2-} + [Ni(en)_3]Cl_2 \xrightarrow{\Delta} 3SO_4^{2-} + NiS \downarrow + 3en + 4S + 2Cl^- \quad (2)$$

$$4S_2O_3^{2-} + [Ni(en)_3]Cl_2 \xrightarrow{\Delta} 3SO_4^{2-} + NiS_2 \downarrow + 3en + 3S + 2Cl^- \quad (3)$$

Since the syntheses of equal quantities of NiS and NiS_2 consume the same quantity of $Na_2S_2O_3 \cdot 5H_2O$, NiS and NiS_2 can be obtained at the same time even at relatively low concentration of $Na_2S_2O_3$. However, NiS_2 gradually converts to NiS typically at the mole ratio of $Na_2S_2O_3$ to $NiCl_2$ of 1.925 due to the lack of

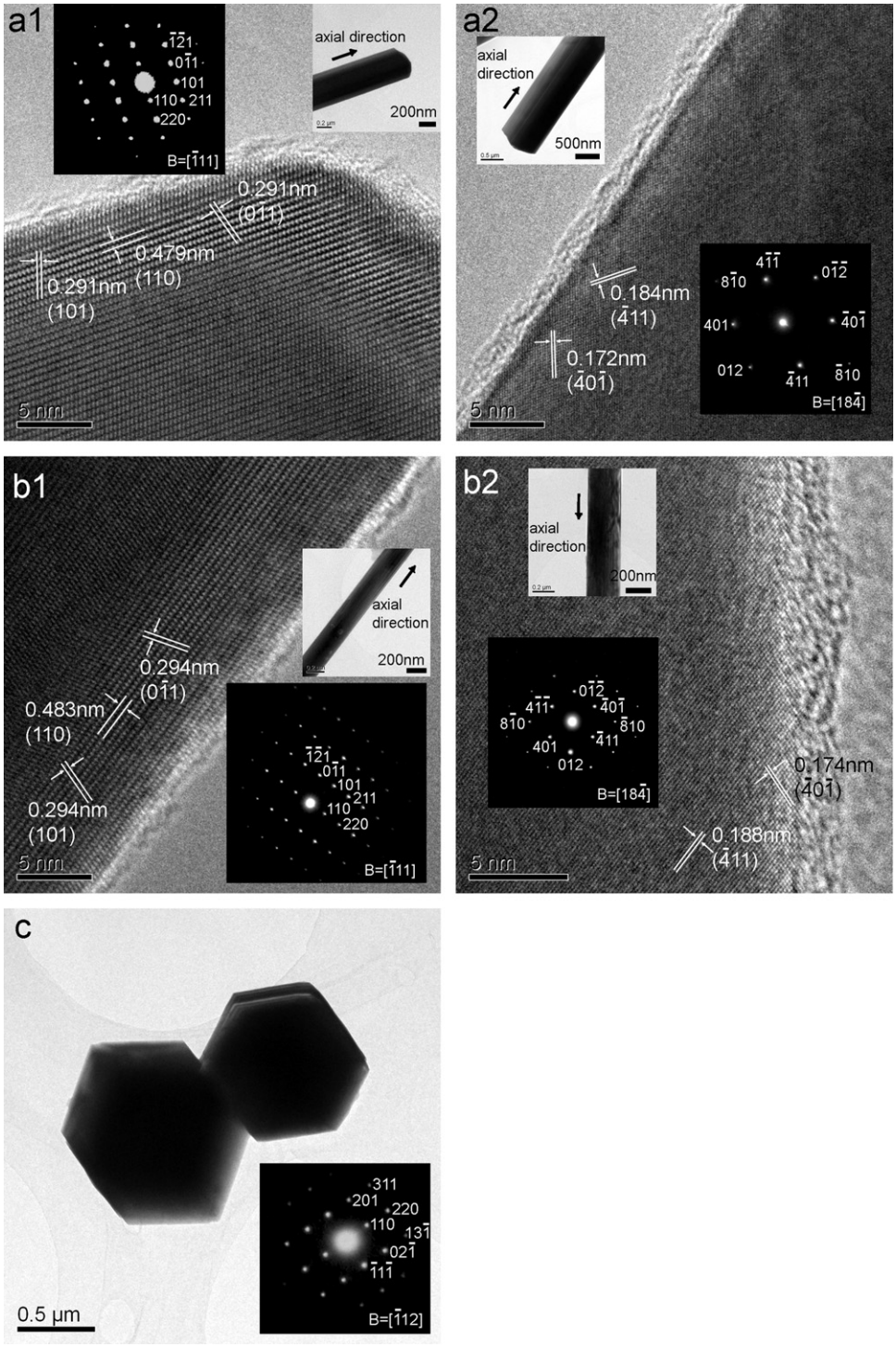

Fig. 3. (a1) and (a2) HRTEM images of r-NiS synthesized at 225 °C for 120 h when the mole ratio of $Na_2S_2O_3$ to $NiCl_2$ is 1.925, the insets showing the corresponding TEM and SAED pattern; (b1) and (b2) HRTEM images of r-NiS synthesized at 200 °C for 60 h when the mole ratio of thiourea to $NiCl_2$ is 2, the insets showing the corresponding TEM and SAED patterns; (c) TEM image of NiS_2 synthesized at 200 °C for 20 h when the mole ratio of $Na_2S_2O_3$ to $NiCl_2$ is 5, the inset showing the SAED pattern of the particle in the upper-right corner.

sulfur source. Pure NiS_2 can be obtained when the sulfur source is superfluous since the occasionally synthesized NiS can further react with S. Considering the synthesis of NiS, NiS nuclei are produced due to the reaction of Ni^{2+} and S^{2-} decomposed from $Na_2S_2O_3 \cdot 5H_2O$ in the solvothermal process. When the nucleus of NiS or NiS_2 forms the nucleus aggregation and the particle growth proceed by consuming smaller particles through a typical Ostwald ripening process, which is similar to the results obtained by Wang et al. [11]. Meanwhile, $[Ni(en)_3]Cl_2$ precipitates gradually disappear at the precipitation–solubility equilibrium. According to the above-mentioned results, the formation processes of r-NiS rods synthesized from $Na_2S_2O_3 \cdot 5H_2O$ are illustrated in Fig. 4d1. Three equivalent crystallographic planes, namely (1 1 0), ($\bar{2}$ 1 0) and (1 $\bar{2}$ 0), homogeneously grow along [1 1 0], [$\bar{1}$ 0 0] and [0 $\bar{1}$ 0] crystallographic orientations, respectively; then the equilateral triangle-like cross-sections are obtained. Attributed to the effects

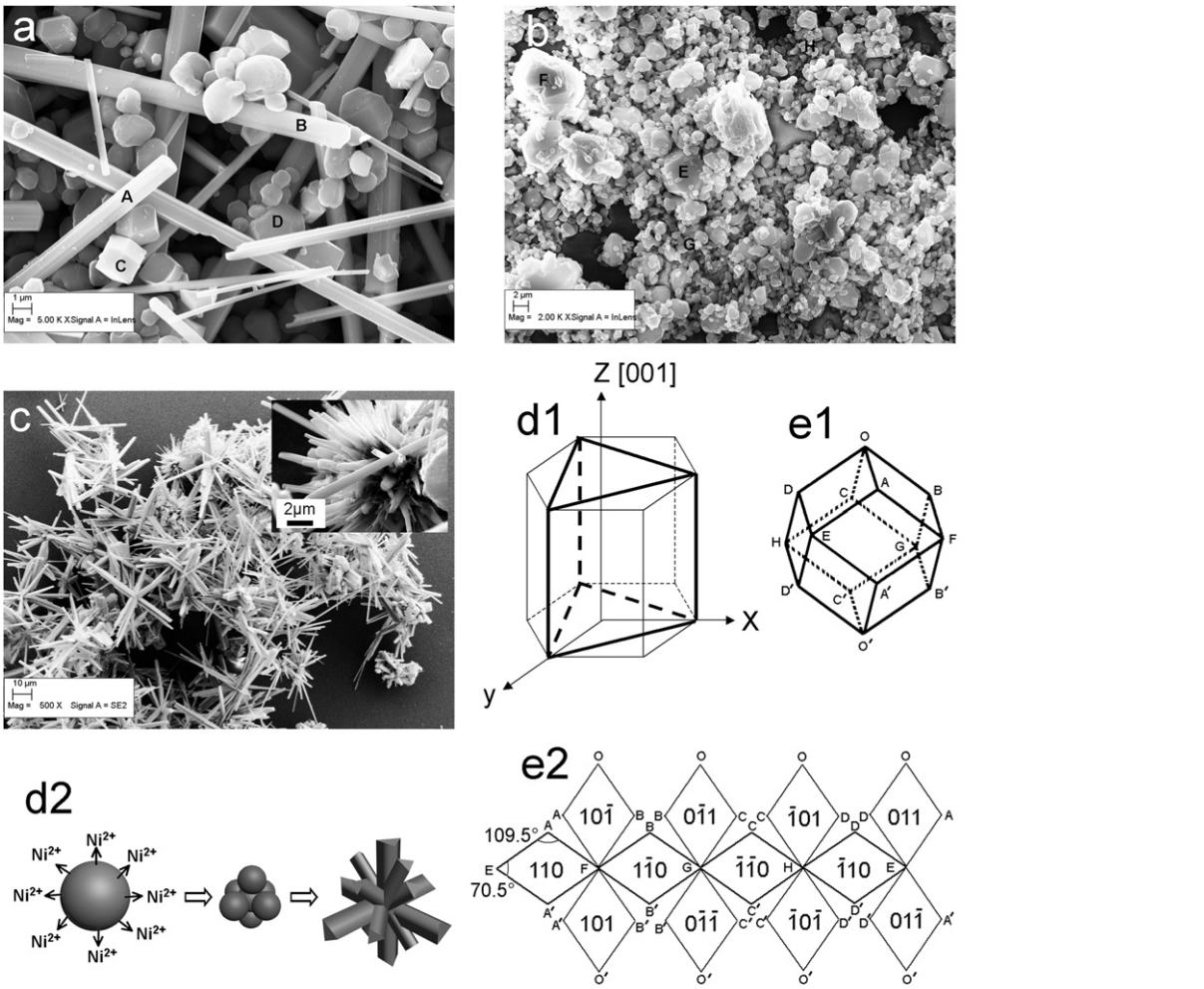

Fig. 4. (a) SEM image of the products synthesized at 225 °C for 20 h when the mole ratio of $Na_2S_2O_3$ to $NiCl_2$ is 1.925; (b) SEM image of the products synthesized at 200 °C for 4 h when the mole ratio of $Na_2S_2O_3$ to $NiCl_2$ is 5; (c) SEM image of the products synthesized at 200 °C for 8 h when the mole ratio of thiourea to $NiCl_2$ is 2, the inset showing the local and detailed configurations; (d1) the anisotropy of r-NiS and schematic view of the formation of equilateral triangle-like cross section of a single r-NiS rod; (d2) schematic view of growth process of r-NiS crystals synthesized from thiourea; (e1) and (e2) schematic view of the formation of rhombic dodecahedron-like NiS_2 crystal.

of bidentate ligand ethylenediamine [18] and the anisotropy of hexagonal crystal structure, the dense-packing crystallographic plane, (0 0 1), of r-NiS grows along *c*-axis to a rod-like morphology. For the reasons of equal crystal orientations and decreasing surface energy the rods tend to join with each other by two assembly modes, side-by-side and end-to-end; then thicker and longer rods form. So the cross-sections of final r-NiS products exhibit polygons or even irregular shapes. The formation processes of NiS_2 rhombic dodecahedron-like crystals are illustrated in Fig. 4e1 and e2. Twelve equivalent crystallographic planes, namely {1 1 0}, homogeneously grow along dense-packing crystallographic orientations, $\langle 1\,1\,0 \rangle$, of face-centered cubic NiS_2 to twelve equivalent rhombic surfaces with two acute angles of 70.5° and two obtuse angles of 109.5°, which is in good accordance with the results of SEM, TEM and SAED analyses.

The purple $[Ni(en)_3]Cl_2$ precipitates dissolve before the precipitation of r-NiS synthesized from thiourea, and the opaque purple slurry changes to transparent solution upon heating. This should be due to the dissolution of $[Ni(en)_3]Cl_2$ and the formation of relatively stable Ni–thiourea complexes, $[Ni(NH_2CSNH_2)_3]^{2+}$. The dissociative thiourea acts as a joint and uses N atoms to form hydrogen bonding (H—N) with H atoms of Ni–thiourea complexes; then several Ni–thiourea complexes aggregate into a group of Ni–thiourea complexes, which is illustrated in Fig. 4d2. Similar to the results obtained by Wang et al. [32] thiourea reacts with H_2O to release S^{2-} slowly upon heating, and the active S^{2-} reacts with Ni^{2+} dissociated from the Ni–thiourea complex upon heating to generate NiS nuclei. Owing to the formation of the group of Ni–thiourea complexes, several NiS nucleus may form on the same group of Ni–thiourea complexes and further aggregate into a group of NiS nucleus. With the slow release of reaction ions, such NiS nuclei grow along the [0 0 1] direction to form rod-like crystals from the core of the group of NiS nucleus; then 3D microstructure are formed. The formation mechanisms of the equilateral triangle-like cross section of r-NiS rod are the same as those of materials synthesized from $Na_2S_2O_3 \cdot 5H_2O$.

In addition, attributed to thermodynamic control after the complete syntheses of h-NiS and r-NiS, h-NiS will gradually convert to the thermodynamically stable r-NiS, which is similar to the results obtained by Zhuang et al. [33]. Similarly, the transformation from NiS_2 to r-NiS (Fig. 1a4) with time extension at temperature higher than 215 °C should be due to the higher thermodynamical stability of r-NiS too.

3.5. Electrochemical property

Fig. 5a shows the discharge capacities vs. cycle number for the r-NiS or NiS_2 electrode using 1 M $LiPF_6$/EC-DMC electrolyte; it can

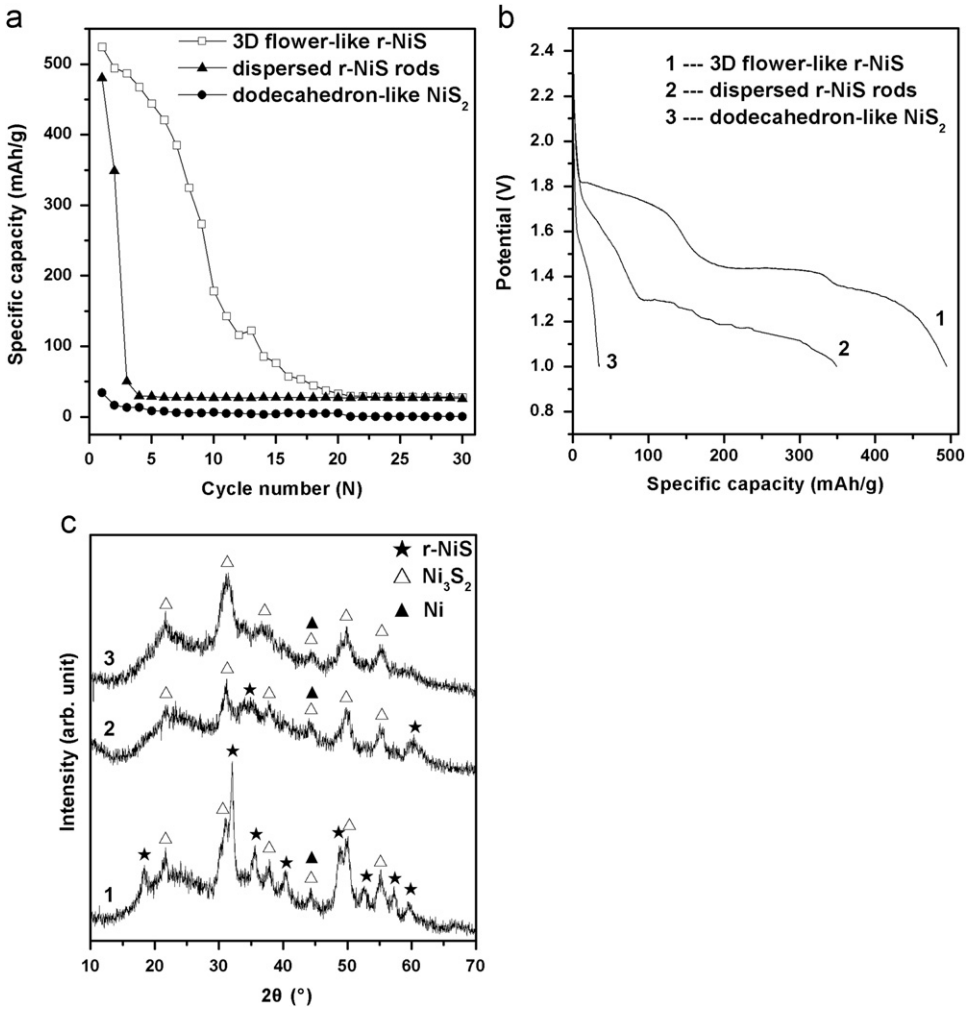

Fig. 5. (a) Discharge capacities vs. cycle number for the r-NiS or NiS_2 electrode using 1 M LiPF6/EC-DMC electrolyte; (b) discharge profiles for the r-NiS or NiS_2 electrode using 1 M LiPF6/EC-DMC electrolyte; (c) XRD patterns of the cathode active materials using dispersed r-NiS as the cathode after 3 charge–discharge cycles (profile 1), and using 3D blossoming flower-like r-NiS as the cathode after 10 charge–discharge cycles (profile 2) and 30 charge–discharge cycles (profile 3).

be seen that the discharge capacity of 3D blossoming flower-like r-NiS microstructures is initially higher than that of dispersed r-NiS rods. The initial discharge capacity of flower-like r-NiS is about 525 mA h/g, which is close to the theoretical capacity of 590 mA h/g [5]. However, NiS_2 hardly shows any discharge capacity (Fig. 5a) and plateau (Fig. 5b) during the whole charge–discharge cycles. The discharge profile of the flower-like r-NiS shown in Fig. 5b exhibits two plateaus; however, only one evident plateau exists in that of the dispersed r-NiS. Moreover the discharge plateau of flower-like r-NiS is about 300–400 mV higher than that of dispersed r-NiS, indicating that the 3D microstructures result in better electroconductivity for supplying more effective and convenient current-carrying paths. It is reported that NiS first converts to Ni_3S_2 and then completely converts to Ni during the course of discharge [5]. Similar results have been obtained in the present work as shown in Fig. 5c, except that a majority of dispersed r-NiS does not convert to Ni_3S_2 and Ni as indicated by the profile 1 in Fig. 5c. The incomplete conversion results in a low discharge capacity of about 50 mA h/g after 3 charge–discharge cycles. Likewise, the discharge capacity decreases remarkably after 10 charge–discharge cycles due to the incomplete conversion of Ni_3S_2 to Ni as indicated by profiles 2 and 3 in Fig. 5c. The reversibility of both r-NiS cathodes in the present work is worse than that of the polycrystalline samples reported in Refs. [5–7], which may be due to the particle size effect, different testing conditions and relatively instable crystal structure. The relatively larger particle size of r-NiS single crystals may result in remarkable anisotropy of electroconductivity, longer current-carrying paths and the incompletion of charge–discharge cycles. A higher temperature of 80 °C is applied to test the charge–discharge cycles of the cells in Ref. [5], which may cause more complete reversible conversions between NiS and Ni compared with our case. The calcined r-NiS powders in Refs. [6,7] possess more stable crystal structure, which is favorable for the charge–discharge cycles.

4. Conclusion

Rhombohedral NiS with dispersed and 3D blossoming flower-like microstructures and NiS_2 crystals with rhombic dodecahedron-like shapes are solvothermal synthesized using enthylenediamine as a solvent. All the products have good single crystalline nature. The purities of r-NiS and NiS_2 crystals synthesized from $NiCl_2 \cdot 6H_2O$ and $Na_2S_2O_3 \cdot 5H_2O$ rely intensively on the reaction temperature, time and the molar ratio of $Na_2S_2O_3$ to $NiCl_2$. The growth mechanism of the flower-like r-NiS microstructures evolving from the group of Ni-thiourea complexes has been proposed. The equilateral triangle-like cross-sections of r-NiS rods are due to three equivalent crystallographic planes, namely (1 1 0), ($\bar{2}$ 1 0)

and $(1\,\bar{2}\,0)$, homogeneously growing along $[1\,1\,0]$, $[\bar{1}\,0\,0]$ and $[0\,\bar{1}\,0]$ crystallographic orientations, respectively. The rhombic dodecahedron-like shapes of NiS_2 crystals are attributed to twelve equivalent crystallographic planes, namely $\{1\,1\,0\}$, homogeneously growing along crystallographic orientations, $\langle 1\,1\,0\rangle$, of face-centered cubic NiS_2. The differences of discharge plateaus and capacities between r-NiS crystals synthesized from two different sulfur sources result from the differences of morphologies. These nickel sulfides with different morphologies may have potential applications in rechargeable lithium batteries, magnetic materials and catalysts, and further studies of their properties are necessary to achieve the goal.

Acknowledgment

The authors are very much grateful to the construct program of the key discipline in Changsha University of Science and Technology, for financial support and giving permission to publish this work.

References

[1] A.P. Alivisatos, Science 271 (1996) 933–937.
[2] X.G. Peng, L. Manna, W.D. Yang, Nature 404 (2000) 59–61.
[3] A. Olivas, J. Cruz-Reyes, M. Avalos, V. Petranovskii, S. Fuentes, Mater. Lett. 38 (1999) 141–144.
[4] A. Olivas, J. Cruz-Reyes, V. Petranovskii, M. Avalos, S. Fuentes, J. Vac. Sci. Technol. A 16 (1998) 3515–3520.
[5] S.C. Han, K.W. Kim, H.J. Ahn, J.H. Ahn, J.Y. Lee, J. Alloys Compd. 361 (2003) 247–251.
[6] J. Wang, S.Y. Chew, D. Wexler, G.X. Wang, S.H. Ng, S. Zhong, H.K. Liu, Electrochem. Commun. 9 (2007) 1877–1880.
[7] T. Matsumura, K. Nakanoa, R. Kanno, A. Hirano, N. Imanishi, Y. Takeda, J. Power Sources 174 (2007) 632–636.
[8] J. Trahan, R.G. Goodrich, S.F. Watkins, Phys. Rev. B 2 (1970) 2859–2863.
[9] D.B. McWhan, M. Marezio, J.P. Remeika, P.D. Darnier, Phys. Rev. B 5 (1972) 2552–2555.
[10] J.H. Jiang, R.L. Yu, R. Yi, W.Q. Qin, G.Z. Qiu, X.H. Liu, J. Alloys Compd. 493 (2010) 529–534.
[11] L.L. Wang, Y.C. Zhu, H.B. Li, Q.W. Li, Y.T. Qian, J. Solid State Chem. 183 (2010) 223–227.
[12] W. Wang, S.Y. Wang, Y.L. Gao, K.Y. Wang, M. Liu, Mater. Sci. Eng. B 133 (2006) 167–171.
[13] D.L. Chen, L. Gao, J. Cryst. Growth 262 (2004) 554–560.
[14] F.M. Zhan, B.Y. Geng, Y.J. Guo, L. Wang, J. Alloys Compd. 482 (2009) L1–L5.
[15] X.M. Zhang, C. Wang, Y. Xie, Y.T. Qian, Mater. Res. Bull. 34 (1999) 1967–1972.
[16] A. Ghezelbash, M.B. Sigman Jr., B.A. Korgel, Nano Lett. 4 (2004) 537–542.
[17] W.Q. Zhang, L.Q. Xu, K.B. Tang, F.Q. Li, Y.T. Qian, Eur. J. Inorg. Chem. (2005) 653–656.
[18] N. Chen, W.Q. Zhang, W.C. Yu, Y.T. Qian, Mater. Lett. 55 (2002) 230–233.
[19] Y.U. Jeong, A. Manthiram, Inorg. Chem. 40 (2001) 73–77.
[20] P.S. Khiew, N.M. Huang, S. Radiman, Md.S. Ahmad, Mater. Lett. 58 (2004) 762–767.
[21] Y. Hu, J.F. Chen, W.M. Chen, X.H. Lin, X.L. Li, Adv. Mater. 15 (2003) 726–729.
[22] X.F. Qian, Y.D. Li, Y. Xie, Y.T. Qian, Mater. Chem. Phys. 66 (2000) 97–99.
[23] G.J. An, C.G. Liu, Y.D. Hou, X.L. Zhang, Y.Q. Liu, Mater. Lett. 62 (2008) 2643–2646.
[24] G.Z. Shen, D. Chen, K.B. Tang, C.H. An, Q. Yang, Y.T. Qian, J. Solid State Chem. 173 (2003) 227–231.
[25] Q.T. Pan, K. Huang, S.B. Ni, F. Yang, D.Y. He, Mater. Res. Bull. 43 (2008) 1440–1447.
[26] Y.H. Zhang, L. Guo, L. He, K. Liu, C.P. Chen, Q. Zhang, Z.Y. Wu, Nanotechnology 18 (2007) 485609.
[27] X.H. Liu, Mater. Sci. Eng. B 119 (2005) 19–24.
[28] Z.Y. Meng, Y.Y. Peng, W.C. Yu, Y.T. Qian, Mater. Chem. Phys. 74 (2002) 230–233.
[29] A. Ghezelbash, B.A. Korgel, Langmuir 21 (2005) 9451–9456.
[30] S.H. Yu, M. Yoshimura, Adv. Funct. Mater. 12 (2002) 277–285.
[31] S.L. Yang, H.B. Yao, M.R. Gao, S.H. Yu, Cryst. Eng. Commun. 11 (2009) 1383–1390.
[32] Q.Q. Wang, G. Xu, G.R. Han, Cryst. Growth Des. 6 (2006) 1776–1780.
[33] Z.B. Zhuang, Q. Peng, J. Zhuang, X. Wang, Y.D. Li, Chem. Eur. J. 12 (2006) 211–217.